UNIVERSITY OF CALIFORNIA,
IRVINE

Carbon Nanotube Thin Film Deposition and Amorphization for Template Synthesis of Graphene Nanoribbons

THESIS

submitted in partial satisfaction of the requirements
for the degree of

MASTER OF SCIENCE

in Materials Science

by

Yimeng Sun

Thesis Committee:
Professor Peter Burke, Ph.D., Chair
Professor James Earthman, Ph.D.
Professor Lizhi Sun, Ph.D.

2015

TABLE OF CONTENTS

LIST OF FIGURES

LIST OF TABLES

ACKNOWLEDGMENTS

I would like to express the greatest appreciation to my committee chair, Professor Peter Burke, who has the attitude and the substance of a genius: he continually and convincingly conveyed a spirit of adventure in regard to research and scholarship, and an excitement in regard to teaching. Without his guidance and persistent help, this dissertation would not have been possible. It was an honor to work for him. I am also grateful to my group mates for all their help and friendships.

I would like to thank my committee members, Professor Earthman and Professor Sun, who have taught me very useful knowledge for my thesis.

I am also extremely thankful of my parents, my family, and my friends for their invaluable support. I would like to particularly express my great appreciation for my mother, who has always been encouraging me to further expand my knowledge and has always been there for me in ups and downs of my life.

ABSTRACT OF THE THESIS

Carbon Nanotube Thin Film Deposition and Amorphization for Template Synthesis of Graphene Nanoribbons

By

Yimeng Sun

Master of Science in Materials Science

University of California, Irvine, 2015

Professor Peter J. Burk, Chair

Graphene nanoribbons (GNRs) have been studied extensively because of their extraordinary electronic properties. Due to the unique relationship of bandgap and physical width, GNRs have become one of the most promising candidates for electronic devices. Current GNR synthesis methods usually incorporate unzipping of carbon nanotubes, which is difficult to control. Template growth synthesis is presented as a novel idea to create GNRs in a controllable manner without using harsh chemicals.

The objective of this project was to learn more about the mechanism and feasibility of template synthesis as a means to produce GNRs. In this project, metallic carbon nanotubes were used as template to synthesize GNRs. First, a thin film of nanotubes was deposited on desired substrates, and then they were subjected to plasma etching to convert into an amorphous structure. The samples were then annealed with and without a carbon source as an attempt to produce GNRs. Atomic force microscopy measurements showed that nanotube height decreased and width increased after annealing, which suggests that a planar structure may have formed, such as graphene. Furthermore, Raman spectroscopy

showed that after annealing, there was a slight increase in the G' peak with respect to the G peak as well as a slight right-shift of the G' band, which both indicate the presence of graphene structure. Future work will be to perform electrical measurements and transmission electron microscopy to further verify the presence of GNRs.

CHAPTER 1: INTRODUCTION

Graphene Nanoribbons

Structure of Graphene Nanoribbons

Graphene, first discovered in 2004, is a single-atom-thick sheet of sp^2-bonded carbon atoms. Ever since its discovery, researchers around the world have been studying its potential for creating novel electronic devices. It is a semiconductor with zero bandgap, linear energy dispersion, phonon-like 2D confined properties, ambipolar charge transport, and a high carrier mobility of 10^4 cm^2/Vs at room temperature. Since large-area graphene is a semimetal, it has zero energy bandgap and cannot be directly used to make transistor devices [1]. In terms of the energy band structure, its valence and conduction bands are cone-shaped and intersect at the K points of the Brillouin zone as shown in Fig. 1.1 [2]. Because of its zero energy bandgap, devices with channels made of large-area graphene are not able to be switched off and are consequently unsuitable for logic applications. However, the graphene band structure can be altered to create a bandgap, such as by applying strain or by biasing a graphene bilayer. Another method to open a bandgap is to constrain large-area graphene in one dimension to form graphene nanoribbons (GNRs).

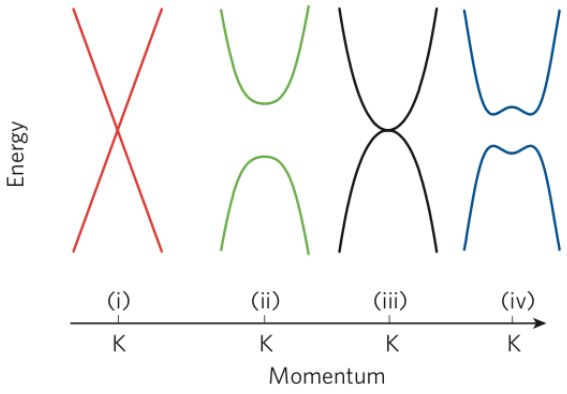

Figure 1.1 Band structure around the K point of (i) large-area graphene, (ii) graphene nanoribbons, (iii) unbiased bilayer graphene, and (iv) bilayer graphene with an applied perpendicular field [2].

GNRs are strips of graphene with an ultra-thin width of less than ten nanometers [3]. There are two types of GNRs: armchair and zigzag, which are distinguished based on their termination style. Figure 1.2 shows the structures of armchair and zigzag GNRs. The width of armchair GNRs is determined by the number of hexagonal carbon rings, which is referred to as dimer lines (N_a) across the ribbon. Similarly, the zigzag GNR width is determined by the number of zigzag chains (N_z) across the ribbon [1]. These termination types also play an important role in determining the electronic states of GNRs. Depending on the width of the GNR, it can be either metallic or semiconducting [4].

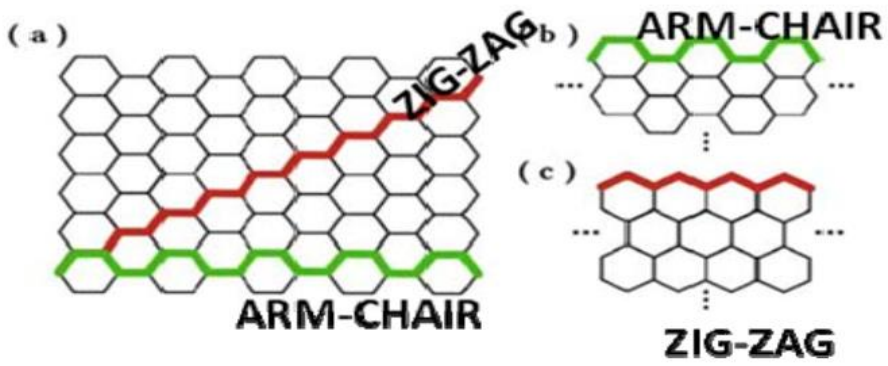

Figure 1.2 (a) Structure of GNRs; (b) Armchair; (c) Zigzag [1].

Applications and Properties of Graphene Nanoribbons

Zigzag GNRs have edge states that are not present in armchair nanoribbons [5-6]. Since these edge states create a flat band around the Fermi level and extend along the ribbon's edge, the GNR may exhibit metallic properties if the width is greater than 10 nm [7-8]. Zigzag GNR edges are highly reactive since there is a high density of states at the edges due to the flat band. By anchoring various atoms or molecules at these reactive edges, it is

possible to modulate the electrical, magnetic, and chemical properties of GNRs. This has many applications for memory devices, sensors, and processing devices [9-11]. Additionally, electronic properties can be modulated by interlayer distance in few-layer graphene. This phenomenon has applications in nano-electromechanical systems (NEMS) [12].

It has been predicted that both armchair and zigzag nanoribbons have a bandgap approximately inversely proportional to its width [13]. The width and structure of armchair GNRs is illustrated in Figure 1.3. GNRs can be engineered with band gaps near that of InN with $E_g \sim 0.7$ eV for GNR widths of approximately 3 nm. Higher bandgaps such as 1.4 eV can be obtained by decreasing the width by 1–2 nm. The formation of a bandgap in GNRs has been shown experimentally for widths down to about 1 nm [14]. Furthermore, theoretical calculations and experiments both have shown bandgaps higher than 0.2 eV for widths below 20 nm as shown in Figure 1.4. As an example of GNR bandgap engineering, if the width of the GNR is designed to be below 10 nm, the bandgap would be large enough to synthesize graphene field effect transistors with on/off ratios of approximately 10^7 at room temperature [15]. In summary, GNRs have unique electronic properties that have the potential as excellent building blocks in future nanoelectronic devices.

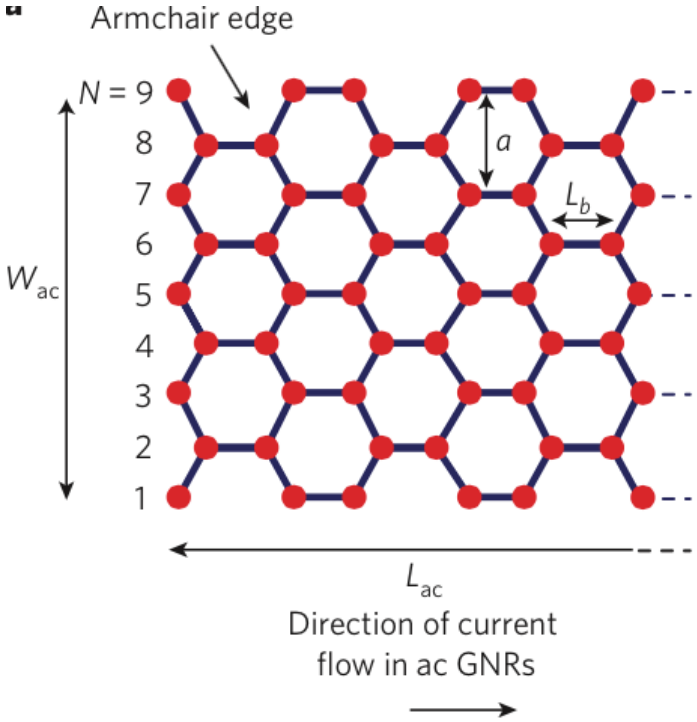

Figure 1.3 Schematic of an armchair (ac) GNR of length L_{ac} and width W_{ac}. The GNR shown here has $N = 9$ carbon atoms along its width and therefore belongs to the $3p$ family, where p is an integer [13].

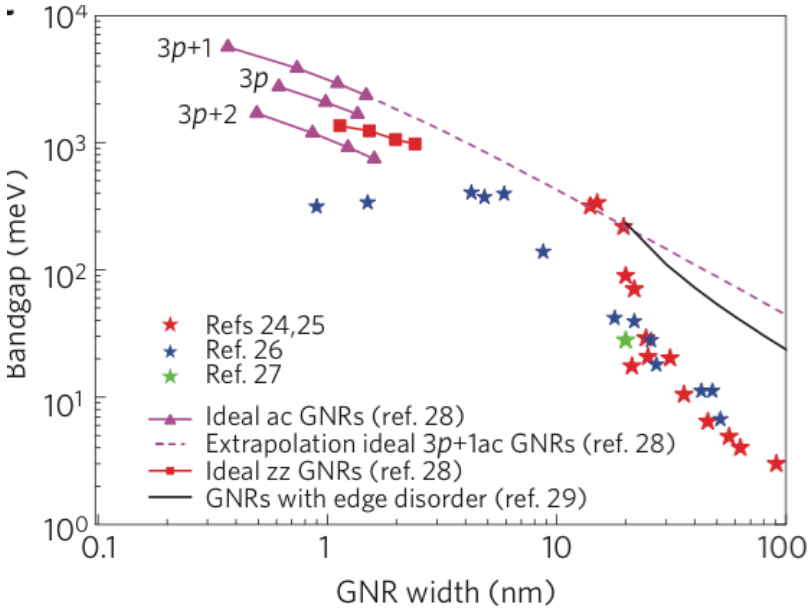

Figure 1.4 Bandgap versus nanoribbon width from experiments and calculations. By comparison, the bandgap of Si is above 1 eV [14],[16].

Graphene Nanoribbon Synthesis Methods

Synthesis of high-quality GNRs with smooth edges and thin, well-defined widths is essential for developing GNR-based electronic and spintronic applications. There are a multitude of GNR synthesis methods, which include CVD, direct chemical synthesis, lithographic patterning followed by plasma etching, sonochemical breaking of chemically-derived graphene, metal-catalyzed or oxidation cutting of graphene, and unzipping of carbon nanotubes (CNTs). Table 1.1 summarizes key details about GNR synthesis methods [17].

Table 1.1 Summary of key GNR synthesis methods [17].

Table 1. Summary of recent experimental methods for GNR synthesis.[a]

Method	*T*	Environment	Yield	Width [nm]	Edge quality	Bandgap	FET on/off ratio	Refs.
Plasma etching of CNTs	N/A	CNTs partially embedded in polymer film	medium (20%)	10–20	high	small	≈10	[28]
Chemical attack on CNTs	≈330 K	H_2SO_4/$KMnO_4$ solution	nearly 100%	100–500	low	metallic	N/A	[29,52]
Intercalation and exfoliation of CNTs	≈300–500 K	solution	high (60%)	100–250	low	N/A	N/A	[53,54]
Metal-catalyzed cutting of CNTs	≈1100 K	Si substrate	low (5%)	15–40	high	N/A	N/A	[61,62]
Sonochemical unzipping of CNTs	N/A	solution	low (2%)	10–30	high	10–15 meV	N/A	[55,56]
Laser irradiation of CNTs	laser energy (≈200–350 mJ)	substrate	high (60%)	60-160	N/A	N/A	N/A	[57]
Electrochemical unzipping of CNTs	N/A	solution	good	70–100	high	N/A	N/A	[58]
Hydrogen treatment and annealing of CNTs	~670–820 K	substrate with Fe catalyst	N/A	N/A	N/A	N/A	N/A	[63]
Unzipping functionalized CNTs by STM tips	N/A	substrate	N/A	N/A	N/A	N/A	N/A	[64]
Electrical unwrapping of CNTs by TEM	≈3000 K	substrate	N/A	~45	low	N/A	N/A	[65]
Patterning and etching of graphene	N/A	Si/SiO_2 substrates	high	6–100	low	0.1–0.5 eV	1.7–160	[20,21,76,77]
Sonochemical breaking of graphene	N/A	solution	low	<10–50	high	>0.1 eV (<10 nm)	$>10^5$ (<10 nm)	[18,19,78]
Metal-catalyzed cutting of graphene	1200–1300 K	Si/SiO_2 substrates	very low	≈10–15	high	N/A	N/A	[22,23,79–83]
Oxidation cutting of graphene	300–350 K	solution	0					[24,84]
CVD	1000–1700 K	templated substrate	high	20–300	low	≈0 V	$10–10^4$	[25,85,86]
Chemical synthesis	500–700 K	solution or Au substrate	N/A	0.18–0.25 nm	high	≈1.6 eV	N/A	[26,27]

[a] N/A: not available.

CNTs are frequently described as rolled-up graphene sheets, so it is quite intuitive to unroll them to create graphene. Figure 1.5 depicts numerous methods of unrolling or unzipping CNTs to create GNRs.

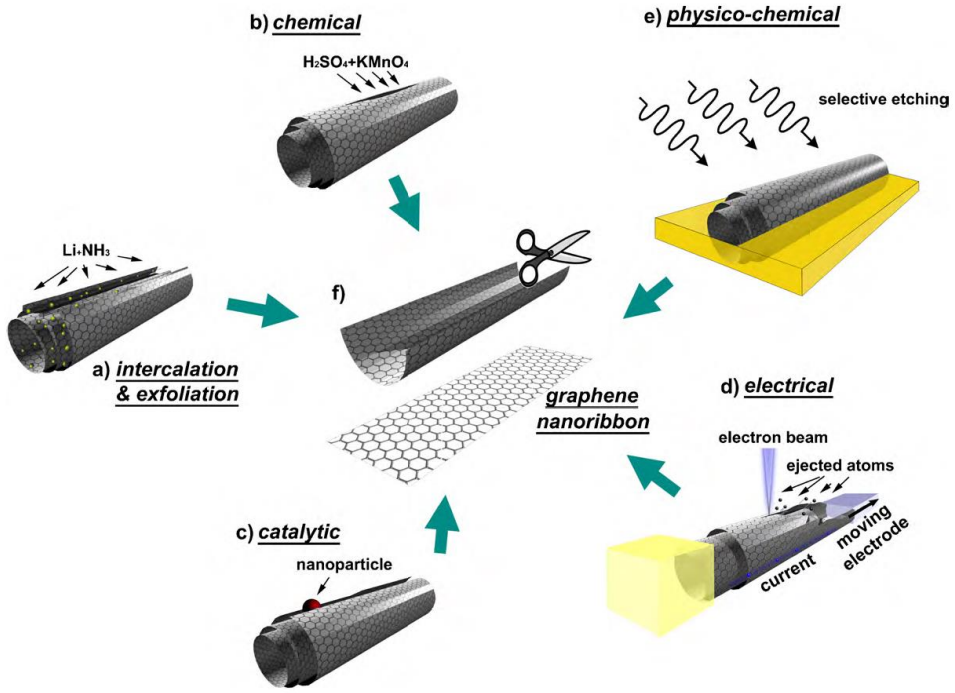

Figure 1.5. Illustration of different ways nanotubes can be unzipped to yield GNRs: (a) intercalation—exfoliation of MWCNTs, involving treatments in liquid NH_3 and Li, and subsequent exfoliation using HCl and heat treatments; (b) chemical route, involving acid reactions that start to break carbon-carbon bonds (e.g. H_2SO_4 and $KMnO_4$ as oxidizing agents); (c) catalytic approach, in which metal nanoparticles "cut" the nanotube longitudinally like a pair of scissors; (d) the electrical method, by passing an electric current through a nanotube, and (e) physicochemical method by embedding the tubes in a polymer matrix followed by Ar plasma treatment. The resulting structures are either GNRs or graphene sheets. [18].

However, chemical unzipping of CNTs usually involves aggressive chemicals, which can lower GNR purity and quality. Furthermore, the number of concentric cylinders and chirality of the CNTs will significantly affect the width, thickness, and edge formation of the

synthesized GNRs. Therefore, it is critical to start with uniform CNTs in order to synthesize high-quality GNRs with smooth edges. Mechanical unzipping of CNTs is another method to produce GNRs, but it usually results in undesirable qualities, such as a lack in width control and high edge roughness. It is also difficult to control the width, edge thickness and thickness of GNRs produced by CVD. The metal nanoparticle cutting method, as shown in Figure 1.5c, is an attractive process because of its simplicity and ability to produce well-defined armchair and zigzag edges. However, it has very low yield, and changes in the cutting direction produce graphene quantum dots instead of GNRs.

One promising method of GNR production is synthesis from templates. Anatoliy and Fung Ling et al. have presented a novel idea about direct growth of aligned GNRs from a DNA template by CVD [19]. It is also reported that Katsuhisa and Tianchen et al. synthesized GNRs from amyloid templates [20]. Thus, template synthesizing of GNRs becomes possible. Carbon nanotubes are a great choice of template because of their narrow width and graphene sp^2 structure. However, since CNTs are quite stable, amorphization is necessary to break down the CNT structure to form a template for GNR growth. After subsequent annealing, the carbon structure is predicted to rearrange and grow to form two dimensional planar structures (GNRs). This method has the potential to produce high-quality GNRs in a straight-forward, reliable process that does not involve hazardous chemicals.

CHAPTER 2: CARBON NANOTUBES

Structure of Carbon Nanotubes

Carbon nanotubes (CNTs) are hollow cylinders consisting of one or more layers of graphene. CNTs can be single-walled (SWNT) or multi-walled (MWNT) as shown in Figure 2.1 [21]. Characteristic qualities of SWNTs and MWNTs are shown in Table 2.1 [22]. The atomic structure of CNTs is well described by a pair of indices (n,m), which define the perimeter of the CNT on the graphene net. The integers n and m designate the number of unit vectors along two directions in the honeycomb crystal lattice of graphene, as shown in Figure 2.2 [23]. If $m = 0$, the nanotubes are known as zigzag nanotubes, and if $n = m$, the nanotubes are called armchair nanotubes. In all other cases, they are chiral nanotubes. Perfectly-structured CNTs have every carbon atom bonded in a hexagonal lattice except at their ends. However, mass-produced CNTs have many defects, such as pentagons, heptagons, and other imperfections in the sidewalls that typically degrade desired properties. SWNTs and MWNTs generally have diameters that are 0.5 to 1.5 nm and 5 to 20 nm, respectively, but MWNT diameters can even exceed 100 nm. CNT lengths range from below 100 nm to several centimeters, and thereby form the bridge between microscopic and macroscopic scales [24].

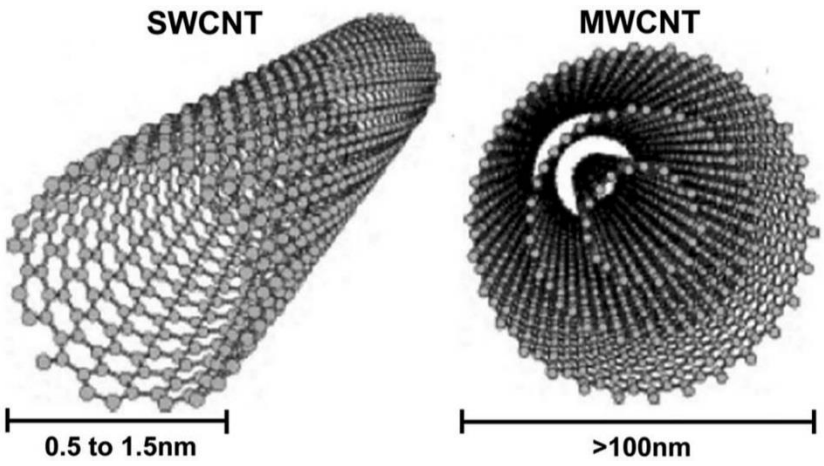

Figure 2.1 Single-wall carbon nanotube and multi-wall carbon nanotube [21].

Table 2.1 Comparison between SWNT and MWNT [22].

Sr. No.	SWNT	MWNT
1.	Single layer of graphene.	Multiple layer of grapheme
2.	Catalyst is required for synthesis.	Can be produced without catalyst.
3.	Bulk synthesis is difficult as it requires proper control over growth and atmospheric condition.	Bulk synthesis is easy.
4.	Purity is poor.	Purity is high.
5.	A chance of defect is more during functionalization.	A chance of defect is less but once occurred it's difficult to improve.
6.	Less accumulation in body.	More accumulation in body.
7.	Characterization and evaluation is easy.	It has very complex structure.
8.	It can be easily twisted and are more pliable.	It can not be easily twisted.

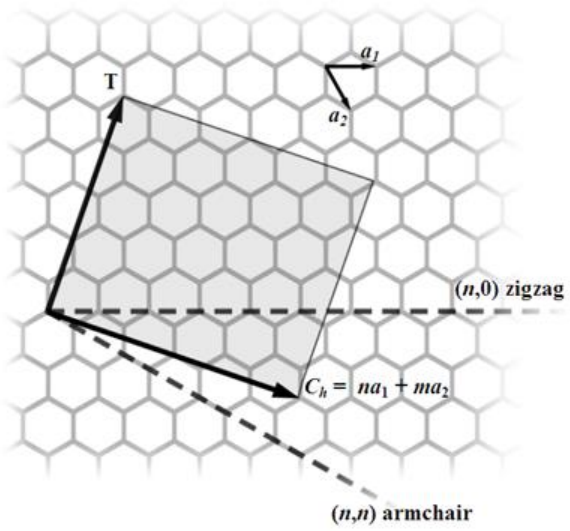

Figure 2.2 The (*n*,*m*) nanotube naming scheme can be thought of as a vector (**C**h) in an infinite graphene sheet that describes how to "roll up" the graphene sheet to make the nanotube. **T** denotes the tube axis, and **a**1 and **a**2 are the unit vectors of graphene in real space [23].

Applications and properties of Carbon Nanotubes

Properties

Mechanical Properties:

Carbon nanotubes have an exceptional combination of stiffness, strength, and tenacity when compared to other fibrous materials, which are typically lacking in one or more of these properties. Furthermore, CNTs are the stiffest and strongest materials yet discovered in terms of elastic modulus and tensile strength, respectively. For example, the experimental specific tensile strength of a single layer in a MWCNT is approximately 100 times that of steel, and the in-plane stiffness of a graphene sheet is comparable to diamond at low strains [25]. Standard SWCNTs can endure a pressure up to 25 GPa without deformation [26].

Electrical Properties:

A nanotube is metallic if it has identical indices $n = m$, and a nanotube is semiconducting with a very small band gap if $n - m$ is a multiple of three. In all other cases, the nanotube is a moderate semiconductor. Therefore, all armchair ($n = m$) nanotubes are metallic, and nanotubes (6,4), (9,1), etc. are semiconducting [27]. Electrons only propagate along the tube's axis because of its nanoscale cross-section. Consequently, carbon nanotubes are commonly referred to as one-dimensional conductors [28].

Thermal Properties:

Carbon nanotubes theoretically have extremely high values of thermal conductivity due to the large phonon mean free path length in sp^2 bond network of CNT walls [29]. Experimental measurements of SWNT thermal conductivity is over 200 W/m K at room temperature and individual MWNTs have values over 3000 W/m K, which is even higher than that for diamond [30].

Applications

Due to the unique electrical and mechanical properties of CNTs, numerous applications have been proposed and range from everyday items such as clothing and sports equipment to combat jackets and space elevators [31]. Nanotube-based transistors, which are also known as carbon nanotube field-effect transistors (CNTFETs), have been designed to operate at room temperature and are capable of digital switching using a single electron [32]. One of the most promising applications of SWNTs is their use in solar panels since they have very strong ultraviolet, visible, and near-infrared absorption characteristics. It has demonstrated that they can produce a substantial increase in efficiency, even at their current nascent state [33]. As another example, the Massachusetts Institute of Technology

Research Laboratory of Electronics uses nanotubes to improve supercapacitors. There are many more applications for CNTs in hydrogen storage, actuators, radar absorption, sensors, electrodes, catalysis, capacitors, and transistors [34-36].

Carbon Nanotube Synthesis Methods

Carbon nanotubes were first produced in high temperature preparation techniques such as arc discharge or laser ablation, but these methods have been replaced by low temperature chemical vapor deposition (CVD) techniques. Low temperature growth below 800 ^{o}C is critical in order to precisely control the alignment, orientation, nanotube length, purity, diameter, and density of CNTs. Non-standard synthesis techniques include liquid pyrolysis and bottom-up organic approach. Figure 2.3 illustrates additional methods for CNT synthesis [37].

Figure 2.3 Currently used methods for Carbon Nanotube synthesis [37]

CHAPTER 3: MATERIALS AND METHODS

Materials

Metallic single-wall carbon nanotube (MSWNT) ink (IsoNanotubes99%, Nanointegris Inc)

Figure 3.1 IsoNanotubes-M-99% MSWNT [38].

MF-Millipore™ Membrane Filters (Pore size: 25nm)

Figure 3.2 MF-Millipore membrane filters [39].

Silicon and Quartz wafers

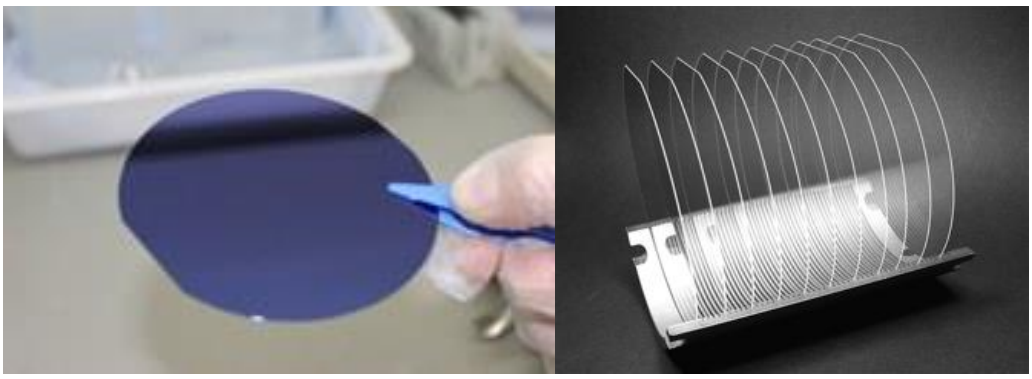

Figure 3.3 Silicon and quartz wafers [40].

Methods

Metallic Carbon Nanotube Thin Film Deposition

Preparation of a Thin Film of Metallic Carbon Nanotubes on an MCE filter:

Metallic carbon nanotube ink was diluted to 1 μg/mL solution with deionized (DI) water. The diluted solution was sonicated for 30min to ensure that the MSWNT solution was uniform. A mixed cellulose ester (MCE) filter was placed in a vacuum filtration apparatus and DI water was added until it covered the MCE filter, as shown in Figure 3.4.

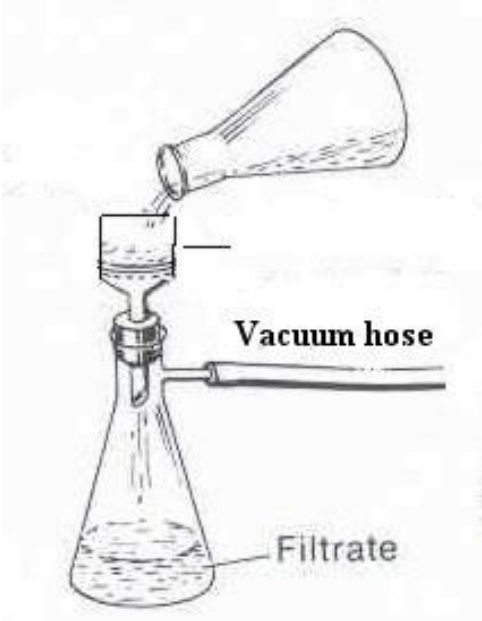

Figure 3.4 Vacuum filtration system [41].

A pipette was used to take 150μL of diluted MSWNT solution and add it into the DI water inside the filtration apparatus. After there was no more liquid passing through the MCE filter, ten additional minutes were allotted for the MSWNTs to form a better bond with the MCE filter. Then, this filtration step was repeated two more times. After the third repetition, fifteen minutes was waited after there was no more liquid passing through the MCE filter. Since the commercial metallic carbon nanotube ink contains surfactant, in order to further purify the deposited carbon nanotube thin film on top of the MCE filter, DI water was added to the vacuum filtration apparatus to wash off residual surfactant. To optimize the cleaning ability, 100mL of DI water was added a total of three times and then the MCE filter was taken out to dry.

Preparation of Substrates:

Silicon and quartz wafers were scribed into 1inch x 2inch substrates. After labelling the backside of each substrate, they were placed in a flat beaker. 70mL of piranha (7:3 H_2SO_4:H_2O_2) was added into the flat beaker and then it was placed onto a 145 ^oC hot plate for 40min. After letting it cool down to room temperature, all of the substrates were rinsed with DI water and blow-dried with nitrogen.

Metallic Carbon Nanotube Thin Film Transfer from MCE Filter to Silicon and Quartz Substrates:

The experimental set-up is shown in Figure 3.5

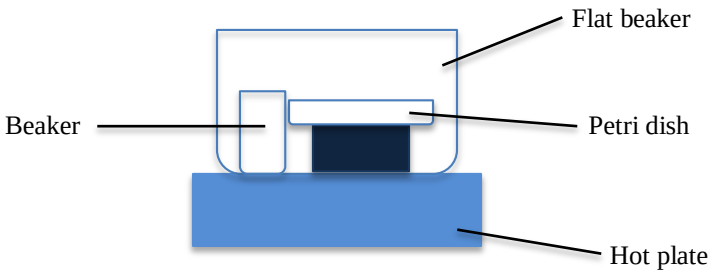

Figure 3.5. Experimental set-up of metallic carbon nanotube thin film transfer from MCE filter to silicon and quartz substrates.

Acetone was added into the flat beaker and the small beaker shown in Figure 3.5, but the Petri dish was kept dry. The hot plate was set to 110 ^oC and adjusted until the acetone started to boil.

The MSWNT-deposited MCE filter was cut equally into four pieces and immersed in ethanol. The wet MCE filters were then put on top of the four substrates while

simultaneously making sure that the MSWNT-deposited side was contacting with the top of the substrates. Gentle pressure was used to press the backside of MCE filters against the substrates so that there were no ripples or bubbles, which meant that the MCE filters were tightly contacting the substrates. Ethanol was continually added onto the MCE filters on top of substrates to make sure the MCE filters were always wet.

The substrates with MCE filters on top were placed into the Petri dish inside the flat beaker, as shown in Figure 3.5. Special attention was made to make sure no liquid acetone nucleated either on top of the samples or anywhere inside the petri dish. If the samples and petri dish were no longer dry, the samples were taken out and dried in air. The entire system was heated up to keep the acetone slightly boiling for one hour in order for acetone vapor to etch some of the MCE filters.

Afterward, the MCE filters became transparent on top of substrates. Four samples were placed inside an acetone stir bath for 25min. The bath temperature was set to 50 ^{o}C and stir speed to 70 RPM.

At this stage, the MCE filters were no longer visible. The four samples were rinsed with methanol and placed inside a methanol stir bath for 20min. The bath temperature and stir speed were the same as the last step.

Lastly, the four samples were taken out and washed with acetone, methanol, isopropyl alcohol, and DI water. Then, they were blow-dried with nitrogen. At this stage, a MSWNT thin film has been deposited on the silicon or quartz substrate.

Plasma Etching

The South Bay Technology Plasma Cleaner in UCI LEXI, as shown in Figure 3.6, was used for this step. The four samples acquired from the last step were placed in the plasma cleaner, and the parameters for Argon plasma etching are shown in Table 3.1.

Figure 3.6. South Bay Technology Plasma Cleaner in UCI LEXI [42]**.**

Table 3.1 Parameters for Ar_2 plasma etching.

Power	Time		
50W	10s	20s	30s
25W	10s	20s	30s

Annealing with and without a Carbon Source

It is well known that copper is a great catalyst for graphene CVD growth [19]. Thus, copper could be helpful for GNR template growth as well. In this experiment, after the samples were plasma etched, they were placed inside a copper foil boat in order to create a catalytic environment. The detailed parameters of the annealing conditions are shown in Table 3.2 and Table 3.3

Table 3.2 Conditions of annealing.

Annealing condition	Silicon substrate	Quartz substrate
Anneal with carbon source	With Cu catalyst	With Cu catalyst
Anneal without carbon source	With Cu catalyst	With Cu catalyst

Table 3.3 Parameters for annealing.

Anneal with carbon source	Anneal without carbon source
1050 °C	1050 °C
1hr	1hr
70mTorr	
H_2 60sccm	
CH_4 30sccm	

Characterization

In this step, the FEI Magellan 400 XHR Scanning Electron Microscope (SEM), PNI Nano-R Atomic Force Microscope (AFM) from UCI LEXI, and Renishaw Raman Microscope from UCI Laser Spectroscopy Facility were used to characterize the samples after each step.

CHAPTER 4: RESULTS

Metallic Carbon Nanotube Thin Film Deposition

Initially, it was very difficult to acquire uniform, large, and clean coverage of carbon nanotube mats. After several adjustments were made to the recipe for CNT deposition, the yield improved from 25% to 100%, which is shown in Table 4.1.

Table 4.1. MSWNT deposition yield.

Trial	SWNT Quantity (μL)	Samples Produced	Yield (%)
1	400	4	25
2	400	8	25
3	400	8	25
4	450	8	50
5	450	4	100

Figure 4.1 and Figure 4.2 are scanning electron microscope (SEM) images of deposited

MSWNT thin film on a silicon substrate. The SEM images indicate that the MSWNT mat is very uniform, clean, and that there is only one layer of MSWNT present on the silicon substrate.

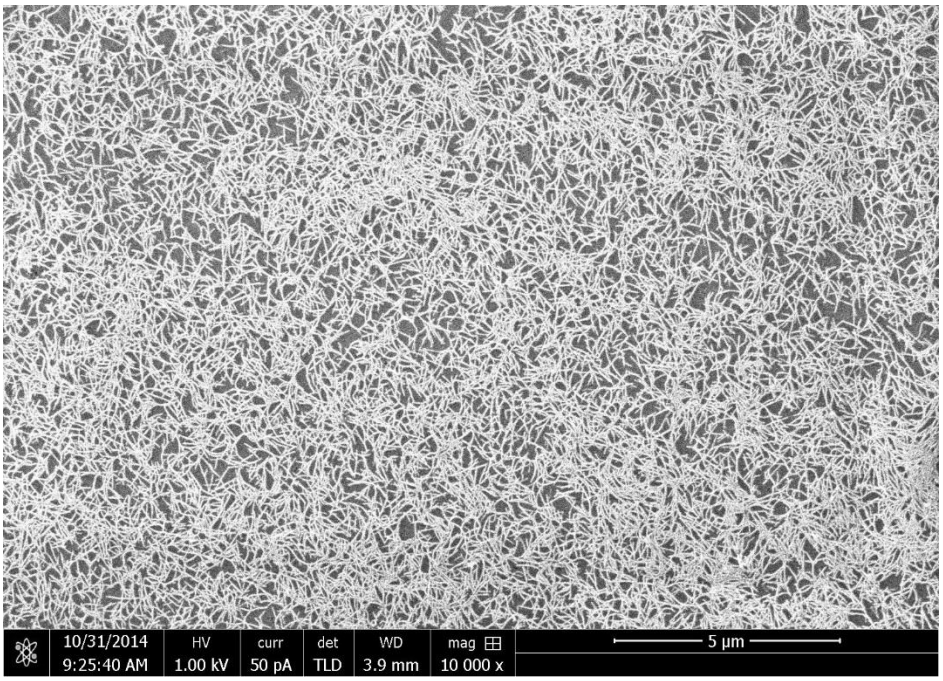

Figure 4.1. High magnification SEM micrograph of 450 µL MSWNT mat.

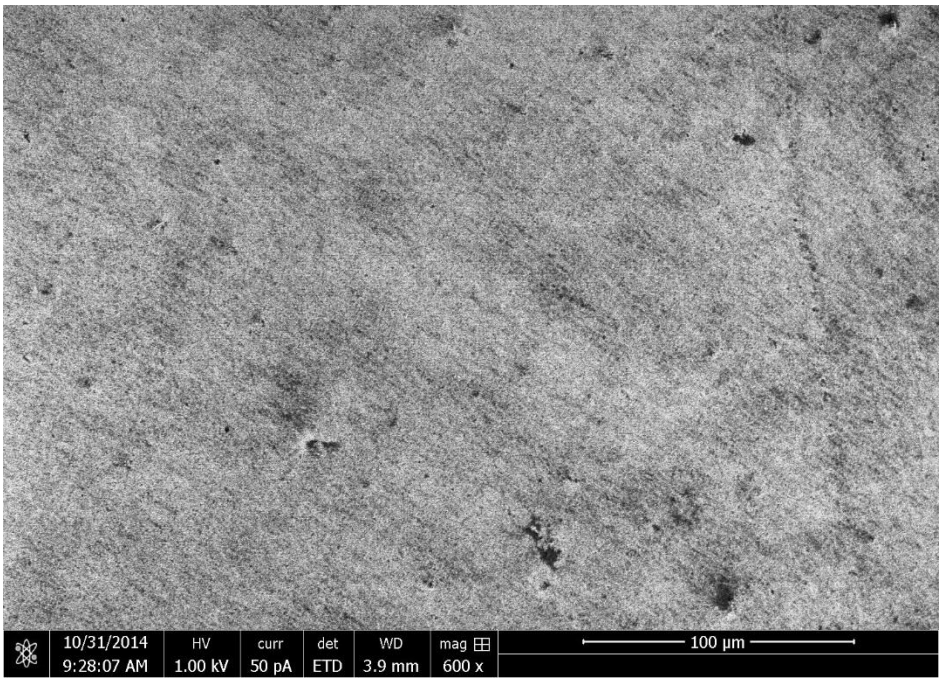

Figure 4.2. Lower magnification SEM micrograph of 450 µL MSWNT mat.

Figure 4.3 is an AFM scan of deposited MSWNT thin film on a silicon substrate. The AFM scan shows that the deposited MSWNT mats have high quality. The height measurements in the AFM scan actually correspond to the MSWNT diameter, and were measured to be 1.063nm. This indicates that only a single monolayer MSWNT was present on the substrate. However, the measured width of 30nm does not seem very reasonable since the width should also correspond to the MSWNT diameter. This anomaly can be explained by the mechanics of AFM measurement, as shown in Figure 4.4. As the AFM tip moves from right to left, it will follow the route shown as the dashed line rather than the solid line since the MSWNTs have very small diameters. Thus, the measured width is much larger than the actual width due to this discrepancy.

(a)

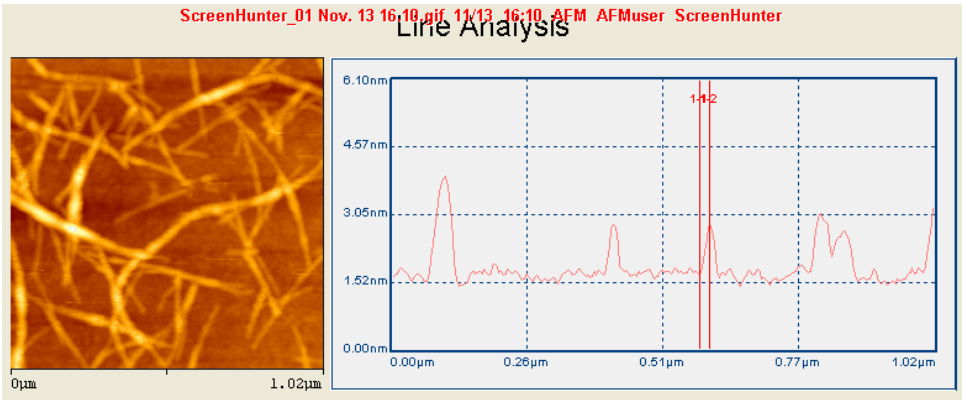

		Pair 1		Pair 2	
		X (μm)	Z (nm)	X (μm)	Z (nm)
Line1	1	0.580	1.706		
	2	0.598	2.769		
	distance	0.019	1.063		
	pt.angle	3.25 °			

(b)

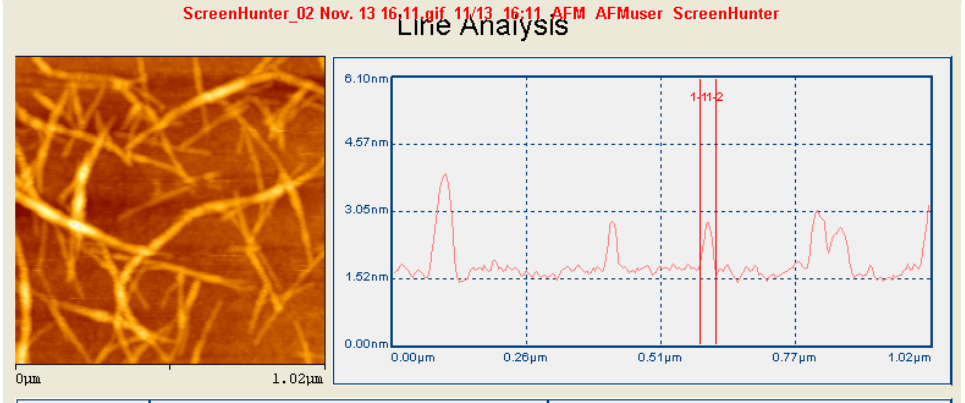

		Pair 1		Pair 2	
		X (μm)	Z (nm)	X (μm)	Z (nm)
Line1	1	0.584	1.782		
	2	0.615	1.735		
	distance	0.030	-0.047		
	pt.angle	-0.09 °			

Figure 4.3. AFM image of 450 μL MSWNT mat showing (a) height measurements and (b) width measurements, which both should correspond to MSWNT diameter.

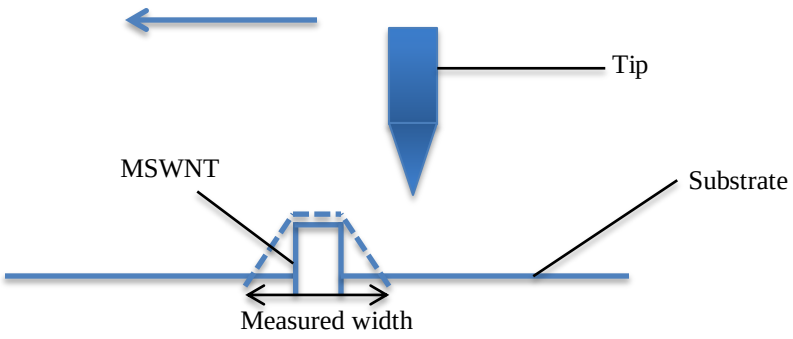

Figure 4.4. Illustration of AFM width measurement overestimation.

Raman Spectroscopy of deposited MSWNT thin film on silicon and quartz substrates is shown in Figure 4.5 and Figure 4.6. In order to minimize the error, six different points on each metallic carbon nanotube mat were chosen with five repeated trials of measurements. The average was taken over all the data points, and the results are shown in Figure 4.5 and Figure 4.6.

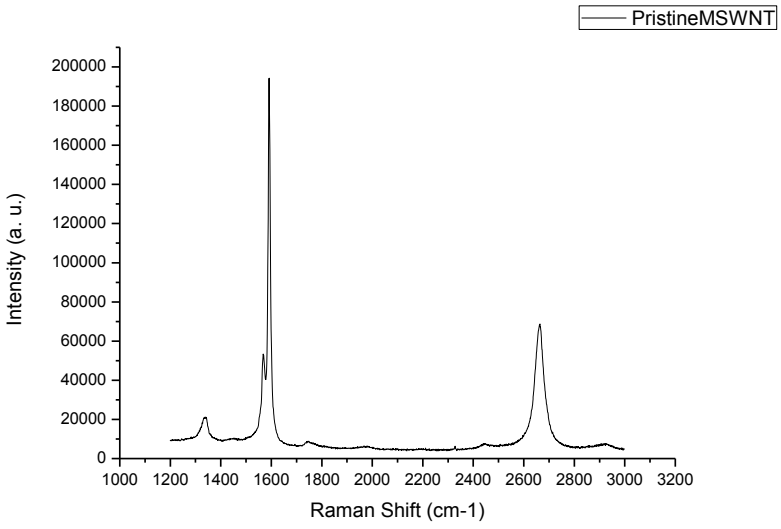

Figure 4.5. Raman spectroscopy of pristine MSWNT on a silicon substrate.

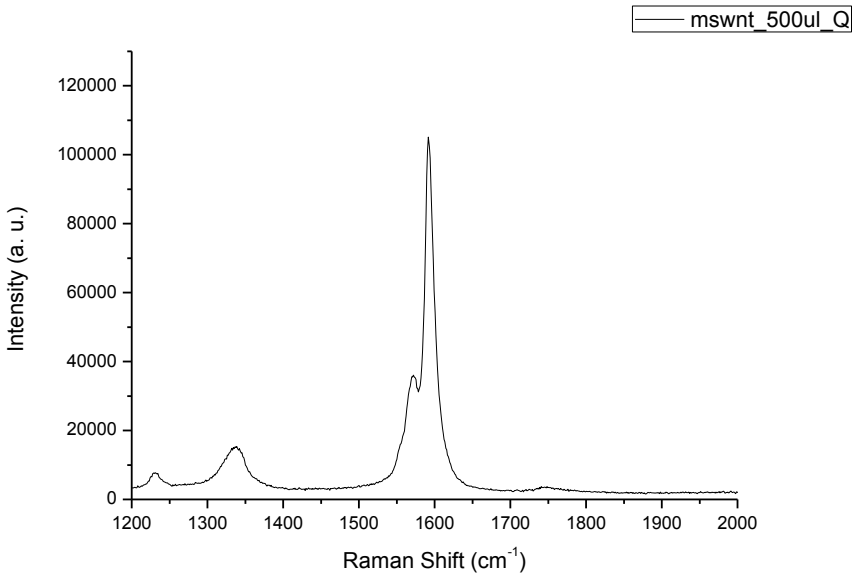

Figure 4.6. Raman Image of pristine MSWNT on quartz substrate.

These figures show that there was a high G peak of approximately 1580cm^{-1} and a small D peak around 1350cm^{-1}. Figure 4.5 also shows a G' peak around 2659cm^{-1}, which is explained by second-order Raman scattering [43].

Plasma Etching

Figure 4.7 shows SEM images of MSWNT after plasma etching. Figure 4.7(a) is an SEM image of MSWNT after 25W plasma etching for 30s. Unlike the uniform monolayer of MSWNT from before, plasma etching caused areas of the substrate to become bare. Additionally, the remaining layers of MSWNTs lost their nanotube structure. In the bare areas of the substrate, there were small nanotube-shaped trenches on the surface. In Figure 4.7(b), almost all of the MSWNTs were etched away and there were barely any MSWNTs left. Thus, 50W power is too high for this step.

(a)

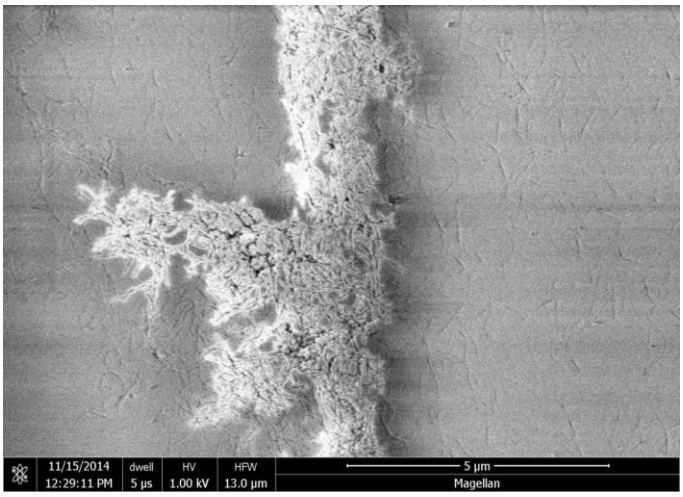

(b)

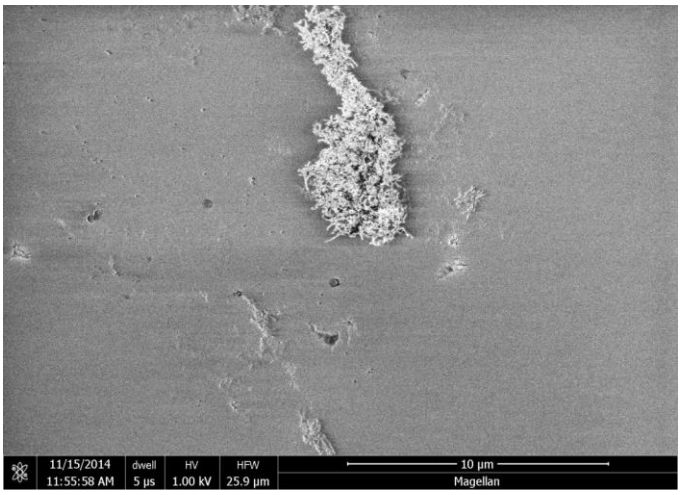

Figure 4.7. SEM images of MSWNT on silicon substrate after plasma etching (a) 25W 30s (b) 50W 30s.

Figure 4.8 shows the AFM images of MSWNT after 10s, 20s, and 30s of 25W plasma etching. The MSWNT structure became more disordered as the plasma etching time was increased. Additionally, the measured thickness in Figure 4.8 (c) was 0.814nm, which is smaller than the thickness of the pristine MSWNT which is around 1nm.

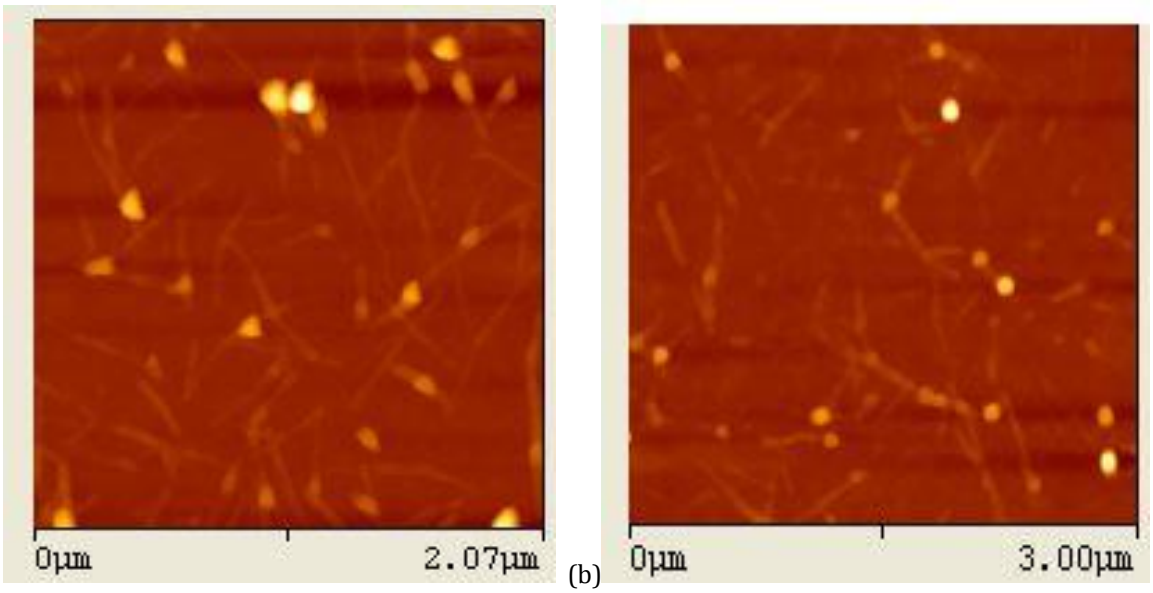

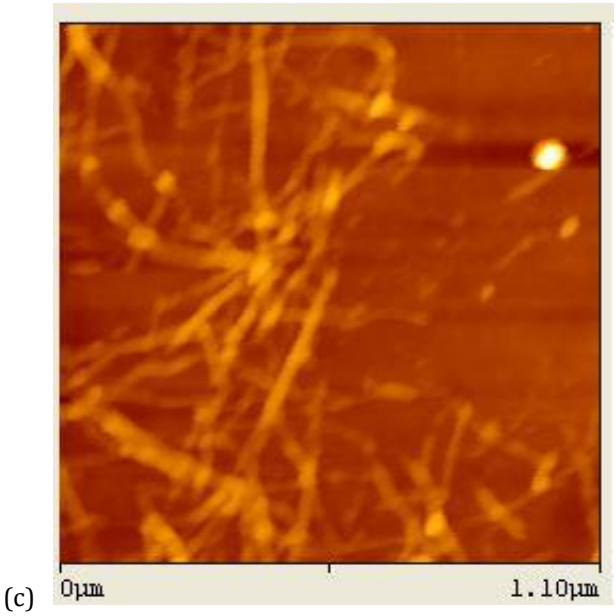

Figure 4.8 AFM images of MSWNT after plasma etching 25W (a) 10s, (b) 20s, and (c) 30s.

Results from Raman spectroscopy are shown in Figure 4.9. It can be seen that the intensity of the D peak relative to the G peak is larger after plasma etching, which indicates that after plasma etching, more structural defects are introduced into MSWNT.

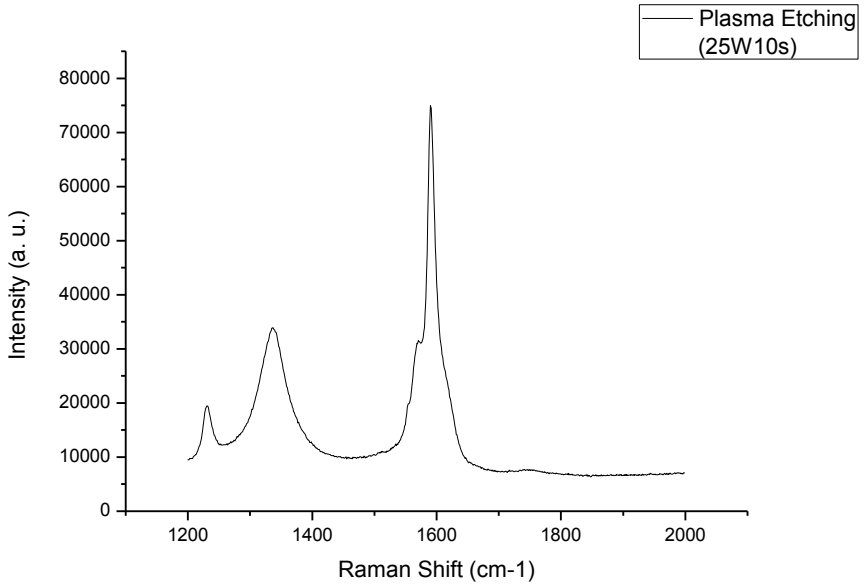

(a)

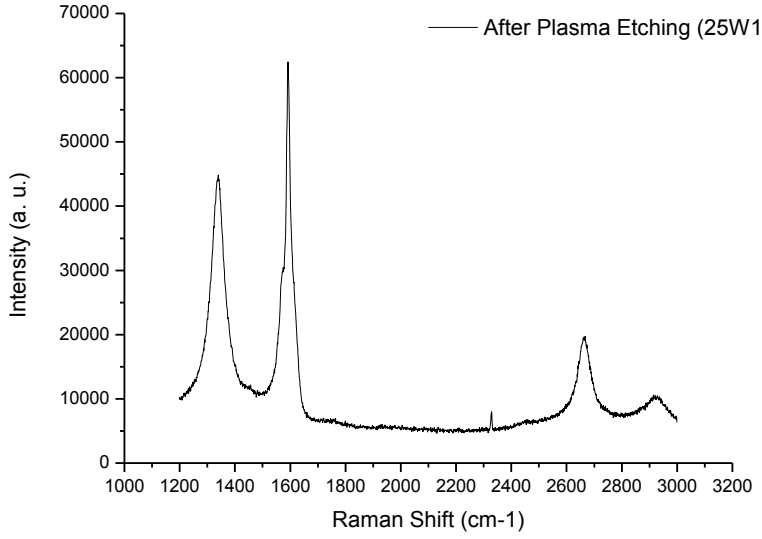

(b)

Figure 4.9. Raman image of MSWNT after plasma etching at 25W for 10s with a substrate made of (a) quartz and (b) silicon substrate.

Anneal with and without Carbon Source

Anneal without Carbon Source (with copper catalyst)

After 1050 ^{o}C annealing of silicon and quartz substrates with plasma-etched MSWNTs atop without a carbon source for 1hr, the surfaces of all the samples were covered with a thin copper film. In order to remove the copper, the samples were immersed inside an ammonium persulfate solution for 30min. After cleaning and drying, some silver-colored dots existed on the surface of the silicon substrates, especially at the corners, which is shown in Figure 4.10. One explanation is that at high temperature, silicon substrates react with copper to form silicon copper oxide.

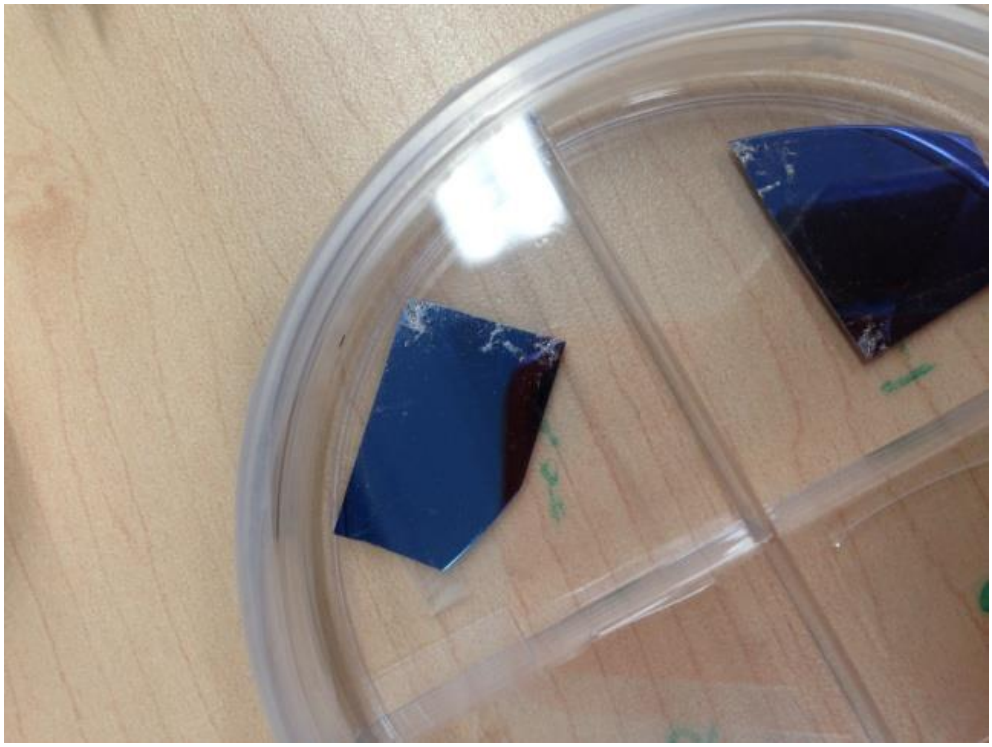

Figure 4.10. Silver-colored dots on silicon substrates after annealing at 1050 ^{o}C for 1hr.

Even though the quartz substrate looked transparent after being soaked inside the ammonium persulfate solution, AFM scans show surface morphology on top of the substrate, as shown in Figure 4.11. This indicates that copper could have reacted with quartz to form a composite material on top.

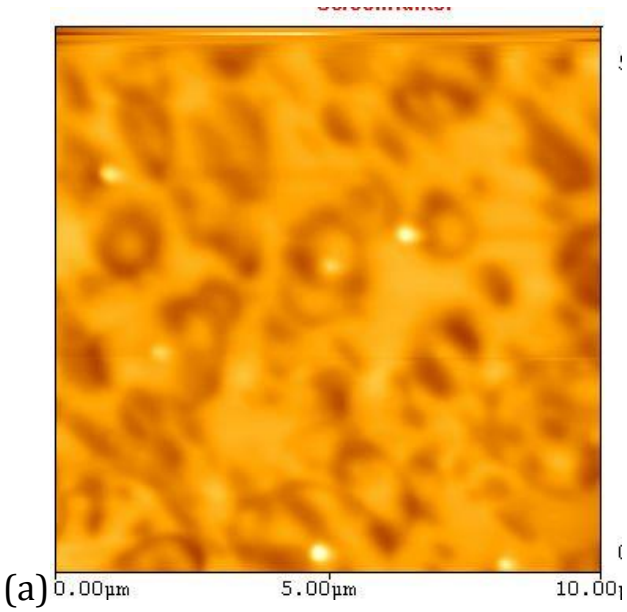

(a)

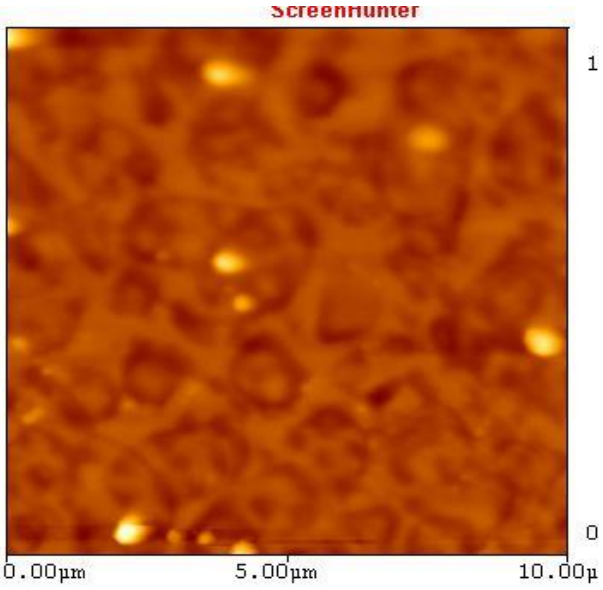

(b)

Figure 4.11. AFM images of MSWNTs after annealing at 1050 °C for 1hr on a quartz substrate and soaking in an ammonium persulfate solution for (a) 30min and (b) 15 hours.

AFM images of MSWNT on silicon substrates after annealing are shown in Figure 4.12.

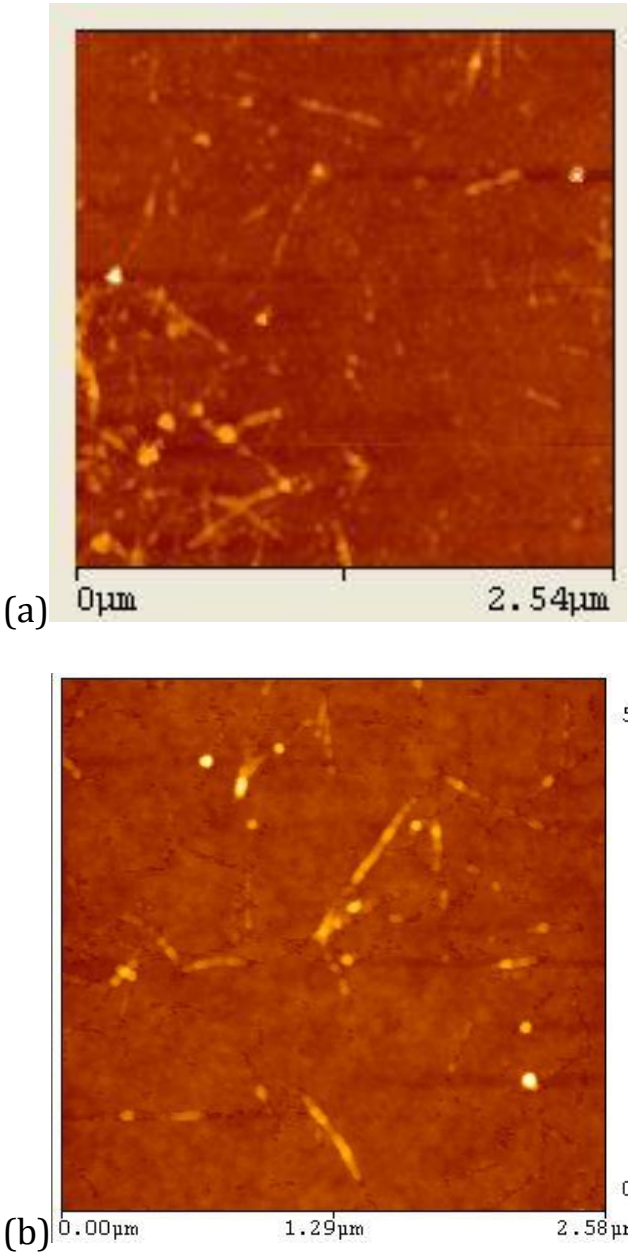

Figure 4.12 AFM images of MSWNT after annealing on silicon substrates after (a) plasma etching at 25W for 10s and (b) plasma etching at 25W for 20s.

From Figure 4.12, it can be seen that after annealing, the MSWNTs are flatter and more 2D-like. Table 4.2 shows the AFM-measured width and height of MSWNTs after annealing on silicon substrates. Based on the table, the height did not change significantly from pristine MSWNT, but the width increased by almost 50%.

Table 4.2. AFM measured width and height of MSWNT after annealing on silicon substrate.

Plasma Etching Time (s)	Width (nm)	Height (nm)
10	77	1.28
20	52	1.082

Results from Raman spectroscopy are shown in Figure 4.13. Looking at the graphs, it is seen that after plasma etching, the D peak (1350cm^{-1}) and G' (2657cm^{-1}) peak increase relative to the G peak (1580cm^{-1}). Another interesting observation was that the G' peak shifted slightly to the right after annealing: the pristine G' peak was at 2657cm^{-1} while after annealing, the G' peak became centered at 2667cm^{-1}.

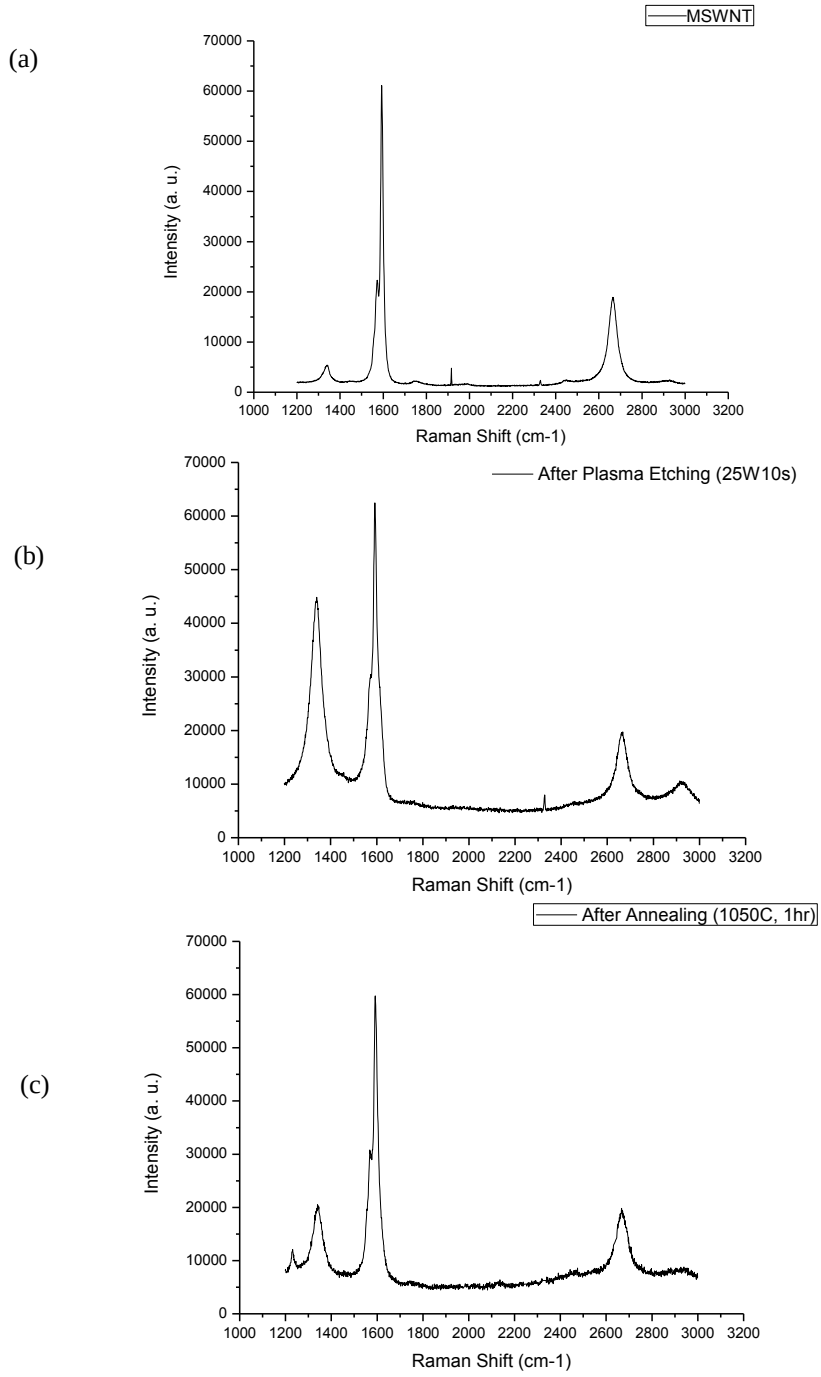

Figure 4.13. Raman spectroscopy of (a) pristine MSWNT on a silicon substrate, (b) MSWNT on a silicon substrate after plasma etching at 25W for 10s, and (c) MSWNT on a silicon substrate after plasma etching at 25W for 10s and annealing at 1050 ^{o}C for 1hr.

Anneal with Carbon Source (with copper catalyst)

Figure 4.14 shows AFM images of MSWNTs on silicon substrates before and after annealing and with different plasma etching times. After annealing with the carbon source, the MSWNTs became flat and wide so that the height decreased while the width increased.

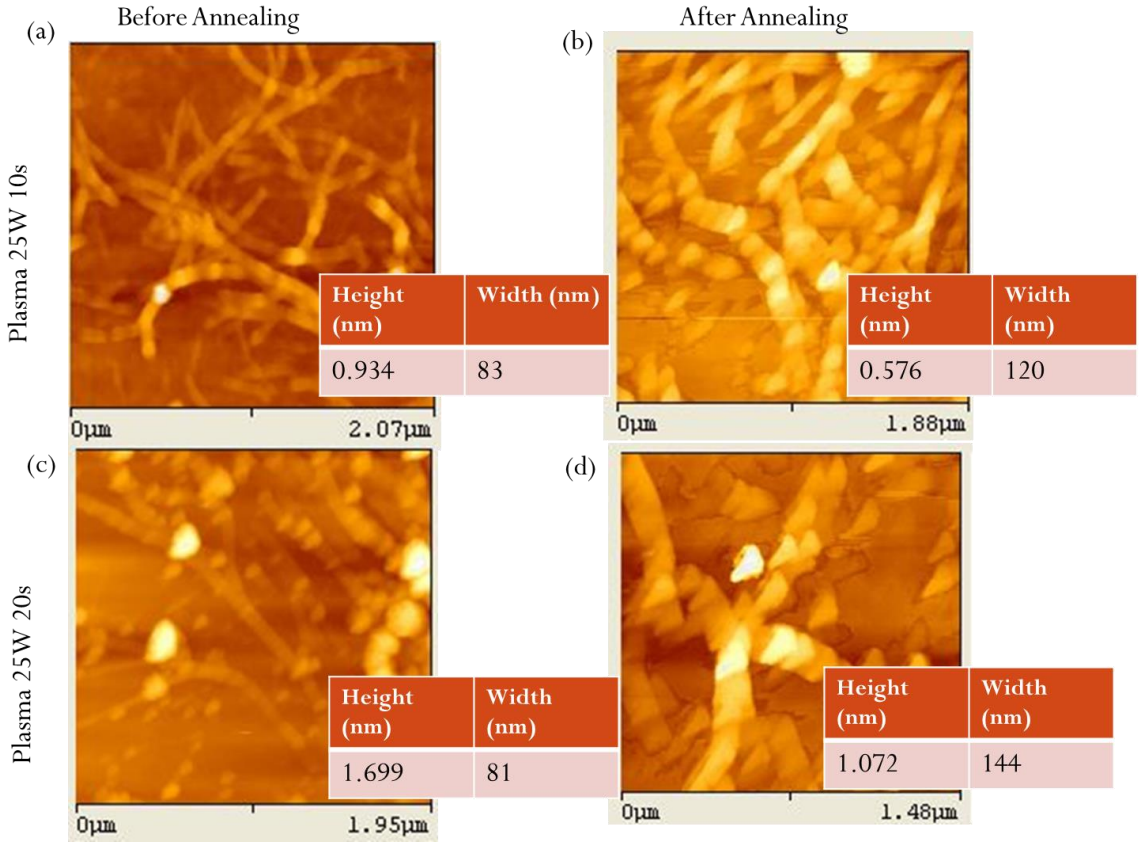

Figure 4.14 AFM images of MSWNT (a) before annealing and after plasma etching at 25W for 10s, (b) MSWNT after annealing and plasma at 25W for 10s, (c) MSWNT before annealing and after plasma at 25W 20s, and (d) MSWNT after annealing and plasma 25W 20s.

Figure 4.15 shows results from Raman spectroscopy. From the graphs, it is seen that after plasma etching, the D peak and G' peak increase relative to the G peak. Another observation was that the G' peak shifted to the right slightly after annealing: the pristine G' peak was about 2659cm^{-1} and shifted to approximately 2669cm^{-1} after annealing.

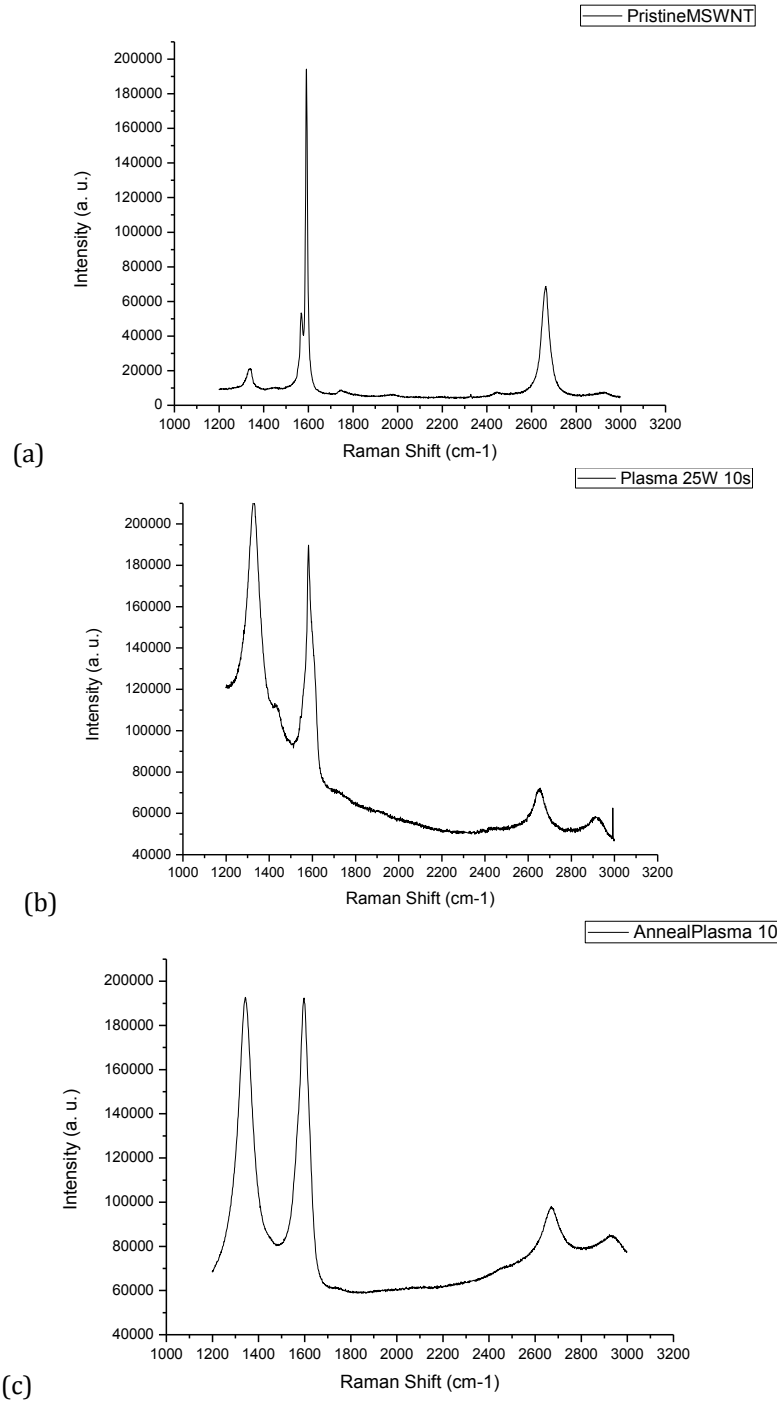

Figure 4.15. Raman spectroscopy of (a) pristine MSWNTs on a quartz substrate, (b) MSWNTs on a quartz substrate after plasma etching at 25W for 10s, (c) MSWNTs on a quartz substrate after plasma etching at 25W for 10s and annealing at1050 ^{o}C for 1hr.

CHAPTER 5: DISCUSSION

As discussed before, studies have shown the great potential of template synthesis of GNRs, such as the direct growth of aligned GNRs from a DNA template and synthesis of GNRs from amyloid templates.[J-K] Similarly, this project aims to produce GNRs by amorphizing MSWNTs and annealing with and without a carbon source. It is hypothesized that the amorphous carbon structure would rearrange to form the 2D sp^2 structure to create GNRs after annealing.

The first step involving MSWNT deposition on silicon and quartz substrates is essential. In order to deposit a clean, uniform monolayer of carbon nanotube film with high yield, several parameters were adjusted, including acetone vapor bath time and temperature, acetone stir bath temperature, stir speed, time, and many others. Finally, high quality MSWNT monolayer thin film was acquired with 100% yield. From the SEM images (Figure 4.1 and Figure 4.2) and AFM images (Figure 4.3), it can be seen that the deposited MSWNT thin film had high quality in terms of uniformity, cleanliness, and widespread coverage. Since the diameter was measured to be 1.063 nm, it indicates that only a single monolayer of MSWNT was present on the substrate. Results from Raman spectroscopy in Figure 4.5 and Figure 4.6 indicate low defect content due to the sharp G peak and small D peak.

After plasma etching, Figure 4.7 (a) shows numerous CNT-shaped trenches in the silicon substrate, which is believed to be caused by substrate etching by MSWNT burning. These trenches may be helpful for GNR template growth since they have the correct shape and could have residual carbon inside the trenches that could act as carbon seeds. However, Figure 4.7 (b) does not show CNT-shaped trenches. One of the reasons that could explain this is because of the very high plasma etching power of 50W which could etch away MSWNTs fast enough without causing indentations in the silicon substrate. Further

experimentation is required to elucidate this phenomenon. Higher plasma etching power also resulted in larger areas of bare substrate after etching. The remaining MSWNTs no longer had characteristic CNT structure, which suggests that the MSWNTs became amorphous. Figure 4.8 shows that longer plasma etching time caused more disordered morphologies, which also suggests conversion to amorphous MSWNTs, but this would need to be studied further for a more definitive conclusion. The results from Raman spectroscopy shown in Figure 4.9 show the increase of the D peak relative to the G peak after plasma etching. This is strong evidence that numerous structural defects were introduced into the MSWNTs after plasma etching, which could suggest an amorphous structure.

From the AFM images of MSWNT after annealing with and without carbon sources (Figure 4.12 and Figure 4.14), it is shown that after annealing, the MSWNT becomes flatter so that the width becomes larger and the height becomes shorter. This implies that 2D structure is generated after annealing, which could be graphene 2D structure. Meanwhile, the results from Raman spectroscopy in Figure 4.13 and Figure 4.15 show that after annealing, the D peak becomes smaller, but not significantly smaller than before. This smaller D peak suggests that annealing helped the structure recover from its amorphous structure to form sp^2 structure. After plasma etching, the D peak could be even smaller, but there are many edges that are counted as defects and compensate for the diminishing D peak. The sp^2 structure suggests that either CNTs or GNRs are present, but since it is especially difficult to grow CNTs without a specific set of conditions, GNRs are more likely. Moreover, there was a slight increase of the G' peak relative to the G peak compared with MSWNTs after plasma etching, as well as the slight right shift of the G' peak compared with pristine MSWNT. Both

these phenomenon illustrate the possibility that graphene structure generated. It has been reported that the G' peak becomes larger as more CNTs are unzipped [44]. It is also known that the G' band for graphene has a slightly larger Raman shift than that of SWNTs [18]. Thus, to some extent, some graphene structure may have been generated after annealing with and without a carbon source.

CHAPTER 6: CONCLUSION

The purpose of this project was to produce GNRs by amorphizing MSWNTs and annealing with and without a carbon source. The process of depositing MSWNTs was optimized to produce a 100% yield in uniform monolayers of MSWNTs. Results from annealing plasma-etched MSWNTs suggest that some degree of GNRs were possibly produced. In support of this claim: 1) AFM scans showed that the MSWNT height decreased and width increased after annealing, which indicates the formation of a planar structure (i.e. graphene), 2) Raman spectroscopy showed that after annealing, there was a slight increase of the G' peak relative to the G peak, and 3) after annealing, there was a slight right-shift of the G' band in Raman spectroscopy, which is characteristic of graphene. These three findings indicate that GNRs could have been obtained, but further testing is necessary to thoroughly evaluate if GNRs were synthesized. Future work will include electrical measurements to test whether there is a significant improvement in the on/off ratio. This would give strong evidence for the existence of GNRs since GNRs have a bandgap while MSWNTs do not. Transmission electron microscopy (TEM) will also be used since it is capable of characterizing GNRs versus MSWNTs. Future work will also include using AFM to characterize the trenches that occurred on the silicon substrate after plasma etching. Additionally, x-ray photoelectron spectroscopy and TEM will be used determine if MSWNTs truly converted into an amorphous structure after plasma etching. Lastly, the presence of copper catalysts during annealing will be tested for the synthesis of GNRs. Template synthesis of GNRs have the potential to revolutionize the manufacturing process. Once GNR synthesis is verified, these structures will be used to create transistors and a myriad of future nanoelectronic devices.

References:

[1] RAECS UIET Panjab University Chandigarh, “”06 – 08 March, 2014: Review of Graphene Nanoribbons A Rising Candidate in VLSI Interconnect Domain

[2] Frank Schwierz, “Graphene transistors,” Nature Nanotechnology 5, 487–496 (2010) doi:10.1038/nnano.2010.89 Published online 30 May 2010

[3] S. Duttaa and S. K. Pati, “Novel properties of graphene nanoribbons: a review,” feature article, Journal of Materials Chemistry, pp. 8207-8223, 29 Jun 2010.

[4] S. Rakheja, V. Kumar, and A. Naeemi, “Evaluation of the potential performance of graphene nano-ribbons as on-chip interconnects,” contributed paper, proceedings of IEEE, vol. 101, no.7, pp. 1740-1765, July 2013

[5] K. Nakada, M. Fujita, G. Dresselhaus, M.S. Dresselhaus, Phys. Rev. B 54 (1996) 17954.

[6] M. Fujita, K. Wakabayashi, K. Nakada, K. Kusakabe, J. Phys. Soc. Jpn. 65 (1996) 19203.

[7] F. Owens, Mol. Phys. 104 (2006) 31079.

[8] L. Yang, C. Park, Y. Son, M.L. Cohen, S.G. Louie, Phys. Rev. Lett. 99 (2007) 186801.

[9] D.W. Boukhvalov, M.I. Katsnelson, Phys. Rev. B 78 (2008) 085413.

[10] B. Huang, Z. Li, Z. Liu, G. Zhou, S. Hao, J. Wu, B. Gu, W. Duan, J. Phys. Chem. C 112 (2008) 1344246.

[11] E. Kan, Z. Li, J. Yang, J.G. Hou, J. Am. Chem. Soc. 130 (2008) 42245.

[12] Y. Guo, W. Guo, C. Chen, Appl. Phys. Lett. 92 (2008) 243101.

[13] Yang, L. et al. Quasiparticle energies and band gaps in graphene nanoribbons.

Phys. Rev. Lett. 99, 186801 (2007).

[14] Chen, Z., Lin, Y-M., Rooks, M. J. & Avouris, Ph. Graphene nano-ribbon electronics. Physica E 40, 228–232 (2007).

[15]. Gogotsi and V. Presser, Carbon Nanomaterials, Second Edition: Taylor & Francis, 2013.

[16] Evaldsson, M., Zozoulenko, I. V., Xu, H. & Heinzel, T, “Edge-disorder-induced Anderson localization and conduction gap in graphene nanoribbons,” Phys. Rev. B 78, 161407 (2008).

[17] L. Ma, J. Wang, F. Ding CHEMPHYSCHEM MINIREVIEWS: Recent Progress and Challenges in Graphene Nanoribbon Synthesis

[18] M. F. L. De Volder, S. H. Tawfick, R. H. Baughman, and A. J. Hart, "Carbon Nanotubes: Present and Future Commercial Applications," Science, vol. 339, pp. 535-539, February 1, 2013 2013.

[19] A. N. Sokolov, F. L. Yap, N. Liu, K. Kim, L. Ci, O. B. Johnson, H. Wang, M. Vosgueritchian, A. L. Koh, J. Chen, J. Park, and Z. Bao, "Direct growth of aligned graphitic nanoribbons from a DNA template by chemical vapour deposition," *Nat Commun,* vol. 4, 2013.

[20] K. Murakami, T. Dong, Y. Kajiwara, "Synthesis of graphene nanoribbons from amyloid temlates by gallium vapor-assisted solid-phase graphitization," *Appl. Phy. Lett,* 104, 243101, 2014.

[21] R. Reilly, "Carbon Nanotubes: Potential Benefits and Risks of Nanotechnology in Nuclear Medicine," J Nuci col. 48 no. 71039-1042, 2007

[22] Asian Journal of Pharmaceutical and Clinical Research Vol.2 Issue 4, October-December 2009: Carbon Nanotubes and Its Applications: A Review Rajashree Hirlekar, Manohar Yamagar, Harshal Garse, Mohit VIJ

[23] Odom et al. Topics Appl. Phys., 2001, 80, 173

[24] Michael F. L. De Volder, Sameh H. Tawfick , "Carbon nanotubes: Present and future commercial applications," SCIENCE VOL 339 1 FEBRUARY 2013

[25] Rodney S. Ruoff, Dong Qian, Wing Kam Liu, "Mechanical properties of carbon nanotubes: theoretical predictions and experimental measurements," Comptes Rendus Physique, Volume 4, Issue 9, November 2003, Pages 993-1008, ISSN 1631-0705

[26] Carbon Nanotube. Available: http://www.nanocyl.com/jp/CNT-Expertise-Centre/Carbon-Nanotubes

[27] Lu, X.; Chen, Z, "Curved Pi-Conjugation, Aromaticity, and the Related Chemistry of Small Fullerenes (C60) and Single-Walled Carbon Nanotubes," Chemical Reviews 105 (10): 3643–3696. 2005

[28] Charlier, J. C.; Roche, S. (2007). "Electronic and transport properties of nanotubes". Reviews of Modern Physics 79 (2): 677. doi:10.1103/RevModPhys.79.677

[29] D. J. Yang, Q. Zhang, G. Chen, S. F. Yoon, J. Ahn, S. G. Wang, Q. Zhou, Q. Wang, and J. Q. Li, "Thermal conductivity of multiwalled carbon nanotubes," *Physical Review B,* vol. 66, p. 165440, 2002.

[30] J. Hone, "Carbon Nanotubes: Thermal Properties," in *Dekker Encyclopedia of Nanoscience and Nanotechnology, Second Edition*. vol. null, ed: Taylor & Francis, 2009, pp. 736-743.

[31] Edwards, Brad C. (2003). The Space Elevator. BC Edwards. ISBN 0-9746517-1-0.

[32] Postma, Henk W. Ch.; Teepen, T; Yao, Z; Grifoni, M; Dekker, C (2001). "Carbon Nanotube Single-Electron Transistors at Room temperature". Science 293 (5527): 76–9. Bibcode:2001Sci...293...76P

[33] "New Flexible Plastic Solar Panels Are Inexpensive And Easy To Make". ScienceDaily. July 19, 2007

[34] Dillon, A. C.; Jones, K. M.; Bekkedahl, T. A.; Kiang, C. H.; Bethune, D. S.; Heben, M. J. (1997). "Storage of hydrogen in single-walled carbon nanotubes". Nature 386 (6623): 377. doi:10.1038/386377a0. edit

[35] Bourzac, Katherine. "Nano Paint Could Make Airplanes Invisible to Radar." Technology Review. MIT, 5 December 2011.

[36] J. M. Schnorr and T. M. Swager, "Emerging Applications of Carbon Nanotubes," *Chemistry of Materials,* vol. 23, pp. 646-657, 2011/02/08 2011.
77, 165427 (2008).

[37] J. Mater. Chem., 2011, 21, 15872: Methods for Carbon nanotubes synthesis-review Jan Prasek, Jana Drbohlavova, Jana Chomoucka, Jaromir Hubalek, Ondrej Jasek

[38] IsoNanotubes-M ™ Metallic SWNTs,
Available:http://www.nanointegris.com/en/metallic-m

[39] Available: http://ecx.images-amazon.com/images/I/71toRnEvzOL.jpg

[40] CUSTOMIZED QUARTZ WAFERS, Available:
http://www.planoptik.com/en/products/quartz_customized.html

[41] Recrystallization and Drying Agents, Available:
http://www.organicchem.org/oc2web/lab/exp/wes/recrystal.html

[42] Available: http://lexi.eng.uci.edu

[43]Andrea C. Ferrari & Denis M. Basko, “Raman spectroscopy as a versatile tool for studying the properties of graphene,” Nature Nanotechnology 8, 235–246 (2013)

[44] S. Jovanocic, T Da Ross, “Raman spectroscopy of graphene nanoribbons synthesized by longitudinal unzipping of multiwall carbon nanotubes,” Phys. Scr. T162 (2014) 014023 (4pp)